IMPACT OF THERMAL RADIATION AND VARIABLE VISCOSITY ON THERMODYNAMIC IRREVERSIBILITY IN CASSON FLUID FLOW OVER A PERMEABLE CONE

Rashmi KRISHNA MURTHY RAO and Nagendramma VELLABOYINA [*]

[1]**Department of Mathematics, Presidency University, Bangalore, India-560064**

[*] Corresponding author; E-mail: nagendramma@presidencyuniversity.in

This article explores how altered viscosity and thermal radiation affect entropy generation in the motion of Casson liquid past a permeable cone. The hydrodynamic behaviour is assumed to be uniform, steady, incompressible boundary layer flow past a surface and affected by a magnetic field with surface conditions of convective type. The fluid viscosity is given as a temperature-exponentially dependent function, and the Rosseland diffusion approximation for radiative heat transport is used. Similarity transformations are used to reduce the nonlinear momentum, energy, and concentration partial differential equations to a system of ordinary differential equations in coupled forms. The resulting problem is numerically solved by an efficient implicit finite-difference Keller–Box scheme. The effects of pertinent parameters, namely Casson parameter, permeability parameter, radiation parameter, Prandtl number and viscosity variation parameter, are presented through graphs on the velocity, temperature and concentration profiles. Also, the viscous dissipation, thermal diffusion and species diffusion aspects of entropy generation are computed and discussed. The results show that increasing the thermal radiation parameter raises the temperature field and the amount of entropy produced. In contrast, augmenting the viscosity variation and Casson parameters will diminish the thermal gradients and render the process less irreversible. The study provides significant insights into the thermal regulation and increment of non-Newtonian fluid systems in porous and radiative environments.

Keywords*: Thermal radiation, variable viscosity, permeable cone, and Keller box method.*

1. Introduction

It is significant to research how fluids and heat flow along conical surfaces because of numerous applications in thermal and industrial engineering, including metal extrusion, geothermal extraction of energy, polymer processing, and transpiration cooling. Ioan Pop and Tsung–Yenna [1] treated steady two-dimensional boundary layer flow over a cone with constant surface temperature. C.S.K. Raju et. al [2] provided a mathematical model to probe the magnetohydrodynamic ferrofluid flow over a slender cone with heat source/sink. They found that increasing values of volume fraction of ferrous nanoparticles increase the friction factor coefficient and heat transfer rate. Gala M. Mohiddin et. al [3] highlighted the steady non–Newtonian incompressible fluid flow within the conical gap between

rotating surfaces of a cone and disc. Their results reveal that the rotation parameter shows a reduction in effects on both the temperature and radial velocity, whereas enhancing the effect on azimuthal velocity. Ian Halloway and Siva Guru Sritharan [4] developed a numerical method for the conical Euler and ideal magnetohydrodynamic equations, which arise in high-speed aerodynamics and magneto-aerodynamics. The porous cone shape is particularly significant because it has the ability to alter the boundary layer properties through sucking or blowing air through it. You need to know how heat and momentum move through these kinds of flows in order to make good cooling and coating systems. D.S. Swetha et al. Al [5]focused on 2-D MHD flow of frictional Maxwell nanofluid through porous conical geometry with convective boundary conditions. The graphical results conclude that the model involving the fractional technique is superior to the integer one. Gouse Mohidding et al. [6] scrutinized buoyancy-driven unsteady natural convection boundary layer flow over a vertical cone embedded in a non-Darcy isotropic porous regime.

Thermal radiation then becomes the dominant mechanism for heat transfer as the temperature increases. The inclusion of radiative heat effects, which are commonly treated with the Rosseland diffusion approximation, alters the temperature field in the thermal boundary layer significantly. Radiative transfer plays a dominant role in high-temperature applications such as gas turbines, solar collectors, nuclear reactors, and re-entry vehicles, since neglecting radiation may lead to substantial errors in calculated heat transfer rates. E. Ragulkumar et. al [7]explained radiative MHD nanofluid flow over a vertical cone with chemical reaction and mass flux. They found that for enhancing values of the thermal radiation parameter, velocity and temperature profiles increase. Abbas et al.[8] scrutinized water-based tri hybrid nanofluid flow over a vertical cone in the presence of thermal radiation and chemical reaction. They analysed results using Finite difference and Chebyshev- Galerkin methods. The impact of radiative nanofluid and heat transfer flow over a truncated cone in the presence of pressure work was investigated by Mohamed Fathy and Emad A Sayed [9]. Shiva Rao and P. N. Deka explored chemically reactive nanofluid flow over a solid cone through a porous medium under heat generation and suction [10]. A few recent analyses have been carried out to explain the importance of the thermal radiation effect on various flow regimes [11][12][13].

Variable viscosity, which is dependent on the temperature in the region, is another key parameter that influences the behavior of fluids. With an increase in temperature, viscosity typically decreases exponentially. This improves the flow and reduces the shear stresses close to the surface. Adding variable viscosity provides a better representation of thermally sensitive fluid flow. Rushikumar and Sivaraj [14] scrutinized unsteady flow, heat, and mass transfer free convective flow over a moving vertical cone and a float plate with variable viscosity. In the mass transfer, a higher-order chemical reaction is considered. The governing equations are solved numerically using the finite difference method. Palani et. al [15] made a numerical investigation on steady incompressible fluid flow with variable viscosity and thermal diffusivity past a heated vertical cone. The impact of temperature-dependent viscosity and thermal conductivity of a viscous fluid on the flow and heat transfer over a rotating vertical cone is investigated by Malik Hamayan Jamil et. al [16]. The highly non-linear equations are solved using the homotopy analysis method. Hazarika et. al [17]studied an unsteady two-dimensional free convective micropolar fluid with variable viscosity and thermal conductivity over a vertical cone. Zubair Mustafa et. al [18] probed an unsteady MHD nanofluid flow over a cone with variable viscosity and viscous dissipation using the HAM method. They noticed that tangential and azimuthal velocities diminish with increasing values of the variable viscosity parameter, whereas the

temperature of the liquid decreases against the unsteady parameter, but it enhances over the Eckert number.

While a great deal of study has been conducted on boundary-layer flow over cones and non-Newtonian fluids, very little has been done examining how thermal radiation, varying viscosity, and entropy generation interact simultaneously in Casson fluid flow over a permeable cone. Past studies often assumed constant viscosity or ignored radiative heat transfer, thereby limiting their applicability to real engineering systems. The present investigation aims to fill this research gap by analyzing the impact of thermal radiation and temperature-dependent viscosity on entropy generation in Casson fluid flow over a permeable cone. Applying the appropriate similarity transformations, the nonlinear partial differential equations governing how mass, momentum, energy, and concentration are conserved are reduced to a system of coupled ordinary differential equations. The resulting equations are numerically solved using the Keller–Box implicit finite-difference method. This is a very accurate and stable scheme for stiff boundary-layer problems. The impacts of important parameters, namely the Casson parameter, radiation parameter, viscosity variation parameter, Prandtl number, and suction parameter, are discussed in detail on the velocity, temperature, concentration, and entropy generation profiles. The findings are useful for interpreting interaction effects between radiative and viscous characteristics in non-Newtonian fluid queues and enhance thermodynamic optimization of industrial heat transfer equipment associated with porous conical shapes.

2. Mathematical Model:

The problem of a steady, laminar, and axisymmetric boundary layer over the vertical permeable cone in a Casson fluid with relevant heat source/sink, thermal radiation melting surface, and variable viscosity is analyzed. The cone is surmised to be exposed in an unsteady fluid, and the surface is capable of constant suction or injection. The Boussinesq approximation is invoked to account for buoyancy-driven effects, while the Rosseland approximation is used to model radiative heat transfer. Viscosity is assumed to vary linearly with temperature. The base fluid is assumed to be electrically conducting, and the Casson model properly addresses the non-Newtonian characteristic of yield stress. It behaves like an elastic solid at low stresses but flows like a viscous fluid when the applied stress exceeds a critical yield value. The rheological model was originally developed to describe the flow of printing ink and later extended to model blood flow and other biofluids. The rheological equation of Casson fluid can be defined as follows.

$$\tau_{ij} = \begin{cases} 2\left(\mu_B + \frac{P_y}{\sqrt{2\pi}}\right)e_{ij}, & \pi > \pi_c \\ 2\left(\mu_B + \frac{P_y}{\sqrt{2\pi_c}}\right)e_{ij}, & \pi < \pi_c \end{cases} \tag{1}$$

where $\tau_{ij} = e_{ij}e_{ij}$ is the component of the stress tensor, μ_B is the Casson viscosity coefficient, π is the product of the components of the deformation rate tensor with itself, and π_c is the critical value of this product following the non-Newtonian model, and P_y is the yield stress of the fluid. The viscous dissipation and the Joule heating are incorporated into the thermal regime, and a nonlinear energy equation is formulated. The surface of the cone is maintained at a uniformly elevated temperature. T_w and concentration C_w, while the ambient temperature and concentration are T_∞ and C_∞ respectively. Forced convection conditions neglect the influence of body and gravitational forces.

Consider variable viscosity as:

$$\mu = \mu_0 e^{-\xi_1(T-T_\infty)} \tag{2}$$

$$\mu = \mu_0(1 - A\theta) \tag{3}$$

where $A = \xi_1(T_W - T_\infty)$ and μ_0 is the viscosity of the fluid

Under the aforementioned assumptions, the governing boundary layer equations for mass, momentum, energy, and concentration are expressed as:

$$\frac{\partial(ur)}{\partial x} + \frac{\partial(vr)}{\partial y} = 0 \tag{4}$$

$$u\frac{\partial u}{\partial x} + v\frac{\partial u}{\partial y} = \frac{1}{\rho}\left(1 + \frac{1}{\delta}\right)\frac{\partial}{\partial y}\left(\mu_T \frac{\partial u}{\partial y}\right) + g\beta(T - T_\infty)\cos\gamma + g\beta^*(C - C_\infty)\cos\gamma - \frac{\sigma B_0^2}{\rho}u - \frac{\nu}{k_1}u \tag{5}$$

$$u\frac{\partial T}{\partial x} + v\frac{\partial T}{\partial y} = \alpha\frac{\partial^2 T}{\partial y^2} + \frac{\mu}{\rho c_p}\left(\frac{\partial u}{\partial y}\right)^2 + \frac{\sigma B_0^2}{\rho c_p}u^{22} - \frac{1}{\rho c_p}\frac{\partial q_r}{\partial y} \tag{6}$$

$$u\frac{\partial C}{\partial x} + v\frac{\partial C}{\partial y} = D\frac{\partial^2 C}{\partial y^2} \tag{7}$$

The radiative heat flux using the Rosseland approximation can be written

$$q_r = -\frac{4\sigma_s}{3k^*}\frac{\partial T^4}{\partial y} \tag{8}$$

where σ_s is the Stefan-Boltzmann constant and $k^*$is the absorption coefficient and can be written as

$$q_r = -\frac{16\sigma_s T_\infty^3}{3k^*}\frac{\partial^2 T}{\partial y^2} \tag{9}$$

Equation (9) is substituted into the energy equation (6), and the equation becomes as follows.

$$u\frac{\partial T}{\partial x} + v\frac{\partial T}{\partial y} = \alpha\frac{\partial^2 T}{\partial y^2} + \frac{\mu}{\rho c_p}\left(\frac{\partial u}{\partial y}\right)^2 + \frac{\sigma B_0^2}{\rho c_p}u^{22} - \frac{1}{\rho c_p}\frac{16\sigma_s T_\infty^3}{3k^*}\frac{\partial^2 T}{\partial y^2} \tag{10}$$

For a mathematical model to be well-posed, the boundary conditions must be appropriate. The no-slip condition requires that the fluid velocity and normal component at the cone surface $y = 0$ be zero ($u = 0, v = 0$), and that the temperature and concentration be kept at a constant wall temperature and concentration $T = T_w$ and $C = C_w$, The velocity, temperature, and concentration fields asymptotically approach the free stream values, i.e., $u \to 0, T \to T\infty$ and $C \to C\infty$, far from the cone surface as $y \to \infty$ and $v \to \infty$. The physical reality of a stagnating boundary layer away from the solid surface is reflected in these conditions.

$$y = 0 : u = 0, v = 0, T = Tw, C = Cw \tag{11}$$

$$y \to \infty : u = 0, T = T\infty, C = C\infty. \tag{12}$$

Similarity transformations are used to reduce the above system of partial differential equations to a collection of ordinary differential equations (ODEs). To automatically satisfy the continuity equation, a stream function $\psi(x, y)$ and a similarity variable η are defined. The energy equation is normalized by a dimensionless temperature function. $\theta(\eta)$, while velocity components are transformed using the stream function.

$$\eta = \frac{y}{x}(Gr)^{1/4}, \psi = \nu r(Gr)^{1/4} f(\eta), Gr = \frac{g\beta x^3 \cos\gamma(T_w - T_\infty)}{\nu^2}$$
$$\theta = \frac{(T - T_\infty)}{(T_w - T_\infty)}, \phi = \frac{(C - C_\infty)}{(C_w - C_\infty)}, r = x\sin\gamma \tag{13}$$
$$u = \frac{1}{r}\frac{\partial \psi}{\partial y}, v = -\frac{1}{r}\frac{\partial \psi}{\partial x}$$

The dimensionless velocity $f(\eta)$, temperature $\theta(\eta)$, concentration $\phi(\eta)$ and their derivatives are involved in the system of coupled nonlinear ODEs that result from these transformations of the coupled nonlinear PDEs. The magnetic field, Casson parameter, viscous dissipation (via Brinkman number), and Joule heating (via Eckert number) all have an impact on these equations.

$$(1 + \frac{1}{\delta})(1 - A\theta)f'''(\eta) - A\theta'(\eta)f''(\eta) + \frac{7}{4}f(\eta)f''(\eta) - \frac{1}{2}(f'(\eta))^2 + \theta(\eta) + \lambda\phi(\eta) - Mf'(\eta) - Kf'(\eta) = 0 \tag{14}$$

$$\frac{1}{Pr}(1 + Nr)\theta''(\eta) + \frac{7}{4}f(\eta)\theta'(\eta) + MEc(f'(\eta))^2 + Ec(f''(\eta))^2 = 0 \tag{15}$$

$$\frac{1}{\mathrm{Sc}}\phi''(\eta)+\frac{7}{4}\mathrm{f}(\eta)\phi'(\eta)=0 \quad (16)$$

With the boundary conditions

$$\mathrm{f}(\eta)=0,\mathrm{f}'(\eta)=0,\theta(\eta)=1,\phi(\eta)=1\ \text{at}\ \eta=0 \quad (17)$$

$$\mathrm{f}'(\eta)=0\ ,\theta(\eta)=0,\ \phi(\eta)=0\ \ \text{at}\ \eta\to\infty \quad (18)$$

2(a). Entropy Generation Analysis

To evaluate the irreversibility in the flow, entropy generation (S'''_{gen}) is computed using Bejan's method. In the presence of magnetic effects, heat conduction, and diffusion, the dimensional entropy generation rate is:

$$S'''_{gen}=\frac{k}{T_\infty^2}\left(\frac{\partial T}{\partial y}\right)^2+\frac{16\sigma_s T_\infty^3}{3k^* T_\infty^2}\left(\frac{\partial T}{\partial y}\right)^2+\mu\left(1+\frac{1}{\delta}\right)\left(\frac{\partial u}{\partial y}\right)^2+\frac{\sigma \mathrm{B}_0^2}{\mathrm{T}_\infty}\mathrm{u}^2+\frac{\mathrm{RD}}{\mathrm{C}_\infty}\left(\frac{\partial C}{\partial y}\right)^2 \quad (19)$$

The entropy generation number N_g is defined as the ratio of local entropy generation to a reference entropy generation rate:

$$\text{Entropy heat generation}\left(N_g\right)=\frac{\text{volumetric rate of entropy generation}}{\text{usual rate of entropy generation}}=\frac{S'''_{gen}}{S'''_0}$$

$$N_g=\frac{\frac{k}{T_\infty^2}\left(\frac{\partial T}{\partial y}\right)^2+\frac{16\sigma_s T_\infty^3}{3k^* T_\infty^2}\left(\frac{\partial T}{\partial y}\right)^2+\mu\left(1+\frac{1}{\delta}\right)\left(\frac{\partial u}{\partial y}\right)^2+\frac{\sigma \mathrm{B}_0^2}{\mathrm{T}_\infty}\mathrm{u}^2+\frac{\mathrm{RD}}{\mathrm{C}_\infty}\left(\frac{\partial C}{\partial y}\right)^2}{\frac{k(\Delta T)^2}{x^2 T_\infty^2}} \quad (20)$$

The dimensionless entropy generation number N_g is

$$N_g=\mathrm{Gr}^{1/2}\left[(1+Nr)(\theta')^2+\left(1+\frac{1}{\delta}\right)\frac{\mathrm{Br}}{\Omega_1}(\mathrm{f}'')^2+\mathrm{M}*\mathrm{Br}*(\mathrm{f}')^2+\gamma\left(\frac{\Omega_2}{\Omega_1}\right)^2(\phi')^2\right] \quad (21)$$

Where $\mathrm{Br}=\frac{\mu v^2 \mathrm{Gr}}{x^2 \mathrm{k}\Delta \mathrm{T}}$ is the Brinkmann number, $\Omega_1=\frac{\Delta \mathrm{T}}{\mathrm{T}_\infty}$ is the thermal ratio, $\Omega_2=\frac{\Delta \mathrm{C}}{\mathrm{C}_\infty}$ is the Concentration ratio and $\gamma=\frac{\mathrm{RDC}_\infty}{\mathrm{k}}$ is the diffusivity parameter.

In this case, the Grashof number (Gr) is a measure of buoyancy-dominated effects in the flow. On the other hand, other non-dimensional parameters represented by the Brinkman number and thermal and concentration ratios are used to account for different physical aspects in the system.

The Bejan number (Be) is defined as the proportion of entropy generated due to heat and mass transfer relative to the total entropy production. Entropy generation in this system occurs as a result of both thermal and mass transport processes.

$$\text{Bejan number}(Be)=\frac{S_{gen,heat+mass}}{Ng}=\frac{(1+Nr)(\theta\prime)^2++\gamma\left(\frac{\Omega_2}{\Omega_1}\right)^2(\phi\prime)^2}{(1+Nr)(\theta\prime)^2+\left(1+\frac{1}{\delta}\right)\frac{\mathrm{Br}}{\Omega_1}(\mathrm{f}\prime\prime)^2+\mathrm{M}*\mathrm{Br}*(\mathrm{f}\prime)^2+\gamma\left(\frac{\Omega_2}{\Omega_1}\right)^2(\phi\prime)^2} \quad (22)$$

2(b). Implementation of Keller-Box method

For non-linear differential equations, one way to obtain the solution is to linearize the differential equation before it is written in finite-difference form. Starting from a first approximation, higher-order iterates can be obtained by solving the linearized equation. Keller–Box approach (KBM) [19] is employed to solve the model formulas due to its fast convergence. Furthermore, KBM is utilized to approach the localized solution for (14) and (16) with constraints (17) & (18). The procedure of using KBM is as follows:

At the first step, all of the ordinary differential equations (ODEs) should be transformed into 1st-order ODEs (14) to (16), [19]:

Consider the third-order non-linear differential Eq. (14) and the second-order non-linear differential Eqs. (15) and (16) with the boundary conditions Eqs. (17) and (18).

$$f'=p \quad (23)$$

$$f''=p'=q \quad (24)$$

$$\left(1+\frac{1}{\delta}\right)(1-Ag)q'-Atq+\frac{7}{4}fq-\frac{1}{2}p^2+g+\lambda h-(M+k)p=0 \quad (25)$$

$$\mathrm{g}=\theta\ , \quad (26)$$

$$g'=\theta'=\mathrm{t}, \quad (27)$$

$$\frac{1}{\mathrm{Pr}}(1+Nr)\mathrm{t}'+\frac{7}{4}\mathrm{ft}+\mathrm{MEc(B)}^2+\mathrm{Ec(q)}^2=0 \quad (28)$$

$$\emptyset=h, \quad (29)$$

$$h'=n \quad (30)$$

$$\frac{1}{\mathrm{Sc}}\mathrm{n}'+\frac{7}{4}\mathrm{fn}=0 \quad (31)$$

Along with boundary conditions as:

f_0=0, p_0=0, g_0=1, h_0=1, P_j =0, q_j=0, h_j=0 (32)

With employment of the quantities midway between net points, centering about the midpoint and employing Newton's linearization method, differences approximation of
Eqs. (23) to (32) can be respectively written as:

$$\delta f_j - \delta f_{j-1} - \frac{l_j}{2}\left(\delta p_j + \delta p_{j-1}\right) = (r_1)_j \quad (33)$$

$$\partial p_j - \partial p_{j-1} - \frac{l_j}{2}\left(\partial q_j + \partial q_{j-1}\right) = (r_2)_j \quad (34)$$

$$(a_1)_j\delta q_j + (a_2)_j\delta q_{j-1} + (a_3)_j\delta t_j + (a_4)_j\delta t_{j-1} + (a_5)_j\delta f_j + (a_6)_j\delta f_{j-1} + (a_7)_j\delta p_j + (a_8)_j\delta g_{j-1} + (a_9)_j\delta g_j + (a_{10})_j\delta q_{j-1} + (a_{11})_j\delta h_j + (a_{12})_j\delta h_{j-1} = (r_3)_{j-\frac{1}{2}} \quad (35)$$

$$\delta g_j - \delta g_{j-1} - \frac{l_j}{2}\left(\delta t_j + \delta g_{j-1}\right) = (r_4)_{j-\frac{1}{2}} \quad (36)$$

$$(b_1)_j\delta t_j + (b_2)_j\delta t_{j-1} + (b_3)_j\delta f_j + (b_4)_j\delta f_{j-1} + (b_5)_j\delta p_j + (b_6)_j\delta p_{j-1} + (b_7)_j\delta q_j + (b_8)_j\delta g_{j-1} = (r_5)_{j-\frac{1}{2}} \quad (37)$$

$$\delta h_j - \delta h_{j-1} - \frac{l_j}{2}\left(\delta n_j + \delta n_{j-1}\right) = (r_6)_j \quad (38)$$

$$(c_1)_j\delta n_j + (c_2)_j\delta n_{j-1} + (c_3)_j\delta f_j + (c_4)_j\delta f_{j-1} = (r_7)_{j-\frac{1}{2}} \quad (39)$$

The boundary conditions that can be satisfied directly without iterative refinement are restated. These values are strictly maintained during every iteration to ensure numerical accuracy, as presented below.

$$\delta f_0 = 0, \delta p_0 = 0, \delta g_0 = 0, \delta h_0 = 0, \delta p_j = 0, \delta g_j = 0, \delta h_j = 0 \quad (40)$$

2(c). The Arrangement of Difference Equations in Vector Notation/Matrix

A key step is to express the above difference equations in matrix form. Improper formulation can result in a singular system (determinant equal to zero) or poorly conditioned submatrices, causing the solution procedure to fail. In addition, a lack of matrix structure greatly reduces computational efficiency. The matrix representation adopted from [20], [21]is given below.

$$A\delta = r \quad (41)$$

$$[A] = \begin{bmatrix} [A_1][C_1] & \cdots & \cdots \\ [B_2][A_2][C_2] & & \\ \vdots & \ddots & \vdots \\ \vdots & \cdots & [B_{n-1}][A_{n-1}][C_{n-1}] \\ & & [B_n][A_n] \end{bmatrix}, [\delta] = \begin{bmatrix} [\delta_1] \\ [\delta_2] \\ \vdots \\ [\delta_{n-1}] \\ [\delta_n] \end{bmatrix}, , [r] = \begin{bmatrix} [r_1] \\ [r_2] \\ \vdots \\ [r_{n-1}] \\ [r_n] \end{bmatrix} \quad (42)$$

3. Results and Discussion:

The present section elucidates the numerical outcomes obtained for the magnetohydrodynamic boundary-layer flow, heat, and mass transfer characteristics of a viscous fluid over a vertically stretching cone with variable viscosity effects. The coupled, nonlinear similarity equations governing the momentum, energy, and concentration fields are solved numerically using the Keller–box method, which is well known for its stability and second-order accuracy in handling boundary-layer-type problems. The effects of the controlling physical parameters, namely the magnetic parameter, viscosity variation parameter, Prandtl number, Eckert number, Schmidt number, and buoyancy-related parameters, on the velocity, temperature, concentration, and entropy generation profiles are examined in detail.

Table 1 shows a quantitative comparison of the current numerical results from the BVP4C and Keller–Box methods with the published data from Abbas et al. [8] for certain values of the governing parameters. The results show that the two numerical methods used in this study agree very well with each other, which shows that both methods are correct and stable. The Keller–Box solutions closely match those obtained via BVP4C in all cases, with only small differences due to discretization and convergence tolerances.

Table 1 – Comparison of skin friction and Nusselt number for $M = \lambda = Ec = Sc = Br = \gamma = \Omega = \Omega_1 = Nr = A = 0, Gr = 1$ & $\delta \to \infty$

Pr	$f''(0)$		$-\theta'(0)$	
	Abbas et al. [8]	Present Results	Abbas et al. [8]	Present Results
0.1	1.06963	1.069341	0.21859	0.21847
0.7	0.81936	0.819543	0.45105	0.45006
1.0	0.76936	0.770001	0.51037	0.50998
10	0.4877	0.486994	1.03302	1.03105

Numerical computations were carried out after ensuring grid independence and convergence of the iterative scheme. The results are depicted graphically to highlight the impact of each parameter on the flow and thermal behavior, and the underlying physical mechanisms governing the observed trends are considered with appropriate physical justification.

Table 2: *Numerical values of C_f, Nu, Sh, entropy generation, and Bejan number for different values of the controlling parameters .*

A	M	λ	δ		K	Nr	Ec	Sc	C_f	Nu	Sh	N_g	Be
0.2									1.114	0.572480	0.34082	2.7138	0.060382
0.4									1.3208	0.58641	0.35141	3.7544	0.045796
0.6									1.6732	0.60342	0.36544	5.928	0.030711
0.8									2.4844	0.62446	0.38672	12.856	0.015166
	1								1.4697	0.59446	0.35786	4.6114	0.038316
	2								0.96822	0.441	0.26095	2.163	0.044955
	3								0.68934	0.34243	0.19761	1.2248	0.047868
	4								0.52941	0.28978	0.16231	0.82806	0.050705
		1							2.3937	0.68895	0.42366	11.993	0.019789
		2							3.323	0.75184	0.47496	22.93	0.012326
		3							4.1876	0.79069	0.51489	36.274	0.0086177
		4							5.0061	0.81395	0.548	51.722	0.0064046
			0.2						2.1037	0.51608	0.3018	3.1127	0.042783
			0.4						1.767	0.55751	0.3298	3.7803	0.041111
			0.6						1.6163	0.57644	0.34363	4.1641	0.039898
			0.8						1.5282	0.58736	0.35209	4.4227	0.039002
					1				1.2328	0.52301	0.31567	3.2575	0.041986
					2				1.0788	0.47223	0.28489	2.5012	0.041986
					3				0.96961	0.43472	0.26152	2.0252	0.046658
					4				0.88745	0.40604	0.24321	1.6999	0.048493
						1			1.4697	0.59446	0.35786	4.6114	0.038316
						2			1.5332	0.76389	0.37559	5.0206	0.038742
						3			1.5747	0.9124	0.38666	5.2989	0.039275
						4			1.6044	1.0483	0.39433	5.5044	0.039928
							0.5		1.4466	0.58786	0.35204	4.4687	0.038667
							1		1.4213	0.57795	0.34547	4.3142	0.038712
							1.5		1.3995	0.56639	0.33957	4.1811	0.038363
							2		1.3804	0.55341	0.33424	4.065	0.037671
								1	1.4583	0.58984	0.49767	4.5461	0.038265
								2	1.4464	0.58661	0.67191	4.4836	0.038374
								3	1.4395	0.58522	0.79318	4.4509	0.038473
								4	1.4347	0.5844	0.88934	4.4302	0.038546

The influence of the governing parameters on the skin-friction coefficient, Nusselt number, Sherwood number, entropy generation, and Bejan number is summarized in Table 2. An increase in the magnetic parameter $\boldsymbol{M}$significantly reduces $\boldsymbol{C_f, Nu}$, and $\boldsymbol{Sh}$ due to the opposing Lorentz force, while simultaneously lowering entropy generation and increasing the Bejan number, indicating a relative dominance of thermal irreversibility. On the other hand, larger values of the fluid variable viscosity parameter $\boldsymbol{A}$ as well as buoyancy ratio parameter λ elevate significantly the skin friction as well as heat and mass transfer rates, but since this enhancement is associated with a sharp increase in entropy generation and reduction in Bejan number implies dominance of fluid-friction irreversibility. Increasing the Casson parameter reduces wall shear stress but enhances heat and mass transfers and therefore a marginal increase in the entropy generation exists as well as a slightly decrease in the Bejan number. The velocity, thermal, and concentration gradients decrease with an increase in the porosity parameter K, that is suppression of C,Nu,Sh, and entropy generation, which consequently increases the Bejan number.

Thermal radiation ($\boldsymbol{Nr}$) markedly enhances the Nusselt number and moderately increases skin friction and Sherwood number owing to intensified thermal energy transport, which also elevates entropy generation with a slight increase in the Bejan number. Variations in the Schmidt number $\boldsymbol{Sc}$ have a negligible impact on $\boldsymbol{C_f}$, and $\boldsymbol{Nu}$, but significantly increase the Sherwood number due to reduced mass diffusivity, while entropy generation and the Bejan number remain almost unchanged. Increasing the Eckert number diminishes $\boldsymbol{C_f, Nu}$, and $\boldsymbol{Sh}$ as viscous dissipation weakens thermal and solutal gradients, resulting in a marginal reduction in entropy generation and Bejan number. Overall, the results clearly demonstrate that magnetic, porous, and viscous effects suppress transport phenomena, whereas buoyancy, radiation, and viscosity variation enhance transport at the expense of increased thermodynamic irreversibility.

Table 3 – ***Variation of entropy generation and Bejan number with Brinkman number, thermal ratio, concentration ratio, and diffusivity parameters.***

Br	$\boldsymbol{\Omega_1}$	$\boldsymbol{\Omega_2}$	$\boldsymbol{\gamma}$	$\boldsymbol{N_g}$	$\boldsymbol{Be}$
0.1				2.3973	0.073705
0.2				4.6114	0.038316
0.3				6.8256	0.025886
0.4				9.0397	0.019546
	0.5			0.78076	0.2263
	1			0.62877	0.28101
	1.5			0.6208	0.28462
	2			0.64883	0.27232
		0.5		4.6114	0.038316
		1		4.6082	0.038342
		1.5		4.6071	0.038351
		2		4.6066	0.038355
			1	3.2625	0.041922
			2	3.2724	0.041795
			3	3.2824	0.041668
			4	3.2924	0.041542

The influence of the Brinkman number (Br), thermal ratio parameter (Ω_1), concentration ratio parameter (Ω_2), and diffusivity parameter (γ) on entropy generation N_g and Bejan number Be is presented in Table 2. The rise in (Br) leads to a significant increase in entropy generation due to increased viscous dissipation, while the Bejan number decreases monotonically, signifying an increasing dominance of fluid friction irreversibility. The rise in the thermal ratio parameter Ω_1 leads to an initial decrease in entropy generation followed by a slight increase at higher values, indicating the opposing effects of thermal diffusion and viscous dissipation; simultaneously, the Bejan number increases, indicating the dominance of heat transfer irreversibility, followed by a slight decrease. The changes in the concentration ratio parameter Ω_2 produce a negligible effect on entropy generation, accompanied by a slight increase in the Bejan number, indicating the insignificant role of mass diffusion irreversibility. Conversely, the rise in the diffusivity parameter γ produces a gradual increase in entropy generation due to increased diffusive forces, while the Bejan number decreases steadily, indicating an increasing dominance of non-thermal irreversibility mechanisms.

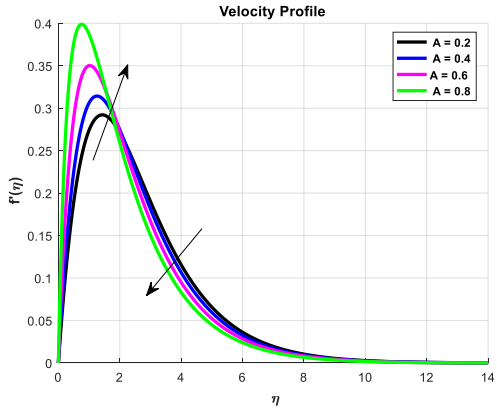

Fig 1. Velocity Profile for different values of A

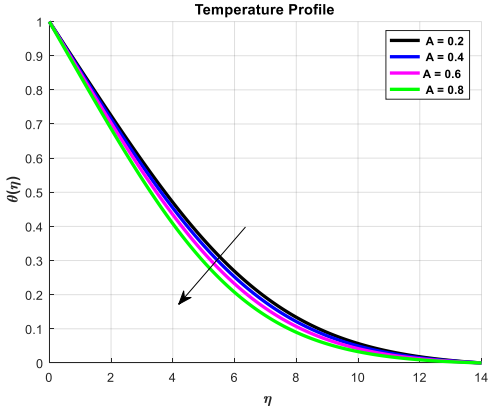

Fig 2. Temperature Profile for different values of A

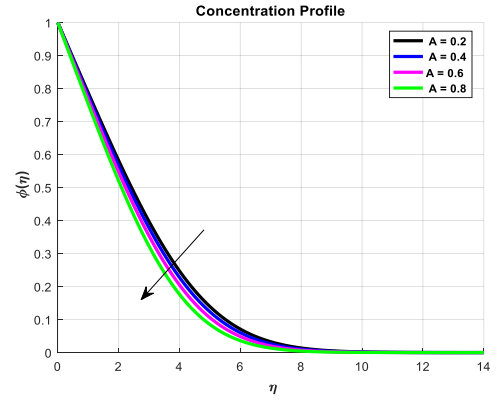

Fig 3. Concentration Profile for different values of A

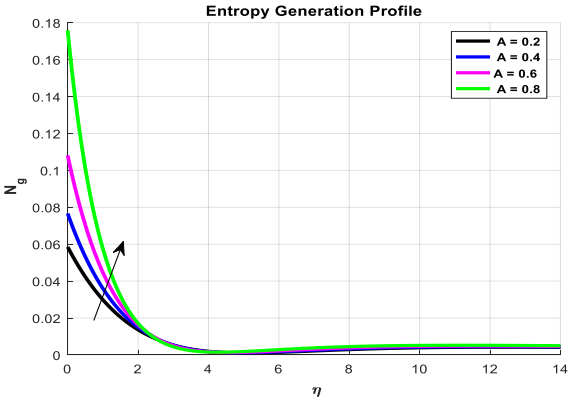

Fig 4. Entropy Generation Profile for different vales of A

The effect of the viscosity variation parameter A, which characterizes the temperature dependence of the fluid's viscosity, is examined for velocity, temperature, concentration, and entropy generation profiles. Figure [1] illustrates the effect of the variable viscosity parameter A on the dimensionless velocity distribution. An increase in A is responsible for the augmentation of the fluid velocity in the region near the surface of the cone, while the change in the velocity near the surface shows a remarkable reduction in the velocity as it gets further away from the surface. The reason for this is the temperature-dependent viscosity of the fluid. The region near the surface of the heated cone experiences higher temperatures, decreasing the value of the viscosity. Therefore, the resistance offered

to the fluid due to this property does not affect the velocity, which gets augmented. On the other hand, as the distance from the surface goes up, the fluid temperature falls, and hence the viscosity goes up. Consequently, the value of the resistance to viscosity will increase, and as a result, the velocity will decrease, and the thickness of the momentum boundary layer will decrease as well. This happens because of the combined effects of a decrease in viscosity near the wall surface and enhanced effects from the viscous forces in the exterior region.

As shown in Figure [2], the temperature within the boundary layer decreases with higher A values. The lower viscosity enhances convective heat transfer, enabling the fluid to carry heat away from the surface more effectively. This, in turn, facilitates thermal mixing and diminishes the width of the thermal boundary layer, resulting in a reduced temperature as it pertains to the entirety. The dependence of the concentration profile on A is shown in Fig. [3]. It is found that with increasing A, the species concentration near the wall diminishes. The stronger fluid flow encourages a more intense convective removal of species from the surface. As a result, species are less retarded on approach to the wall since there is reduced build-up of layers near the surge line, hence thinner concentration boundary layers (CBLs) and lower concentrations. Fig.[4] shows that for increasing values of A, entropy generation increases. As the fluid motion becomes more rapid because of reduced viscosity, it increases velocity gradients inside the boundary layer, leading to higher viscous dissipation, which in turn results in an increase in entropy production.

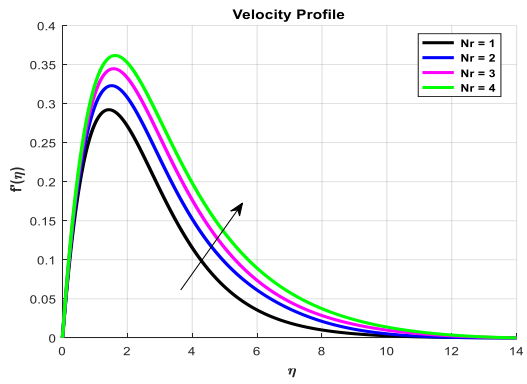

Fig 5. Velocity Profile for different vales of Nr

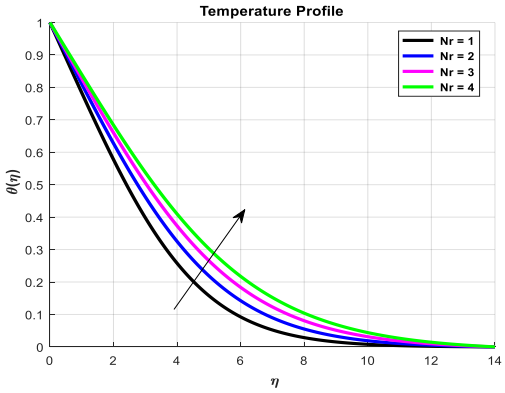

Fig 6. Temperature Profile for different vales of Nr

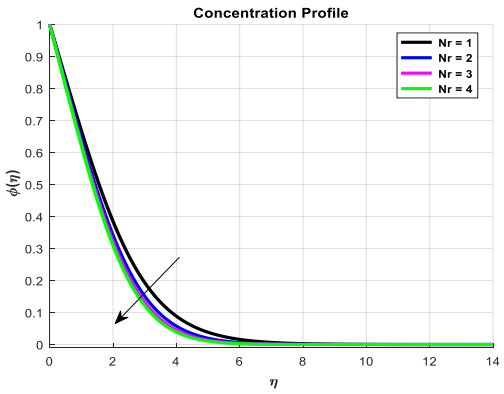

Fig 7. Concentration Profile for different vales of Nr

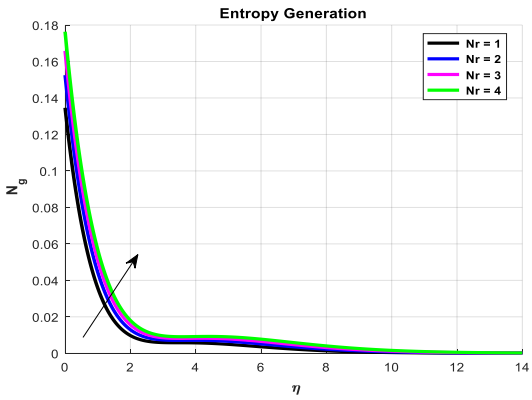

Fig 8. Entropy Generation Profile for different vales of Nr

Figs [5-8] depict the effects of the thermal radiation parameter, Nr, on the velocity, temperature, concentration, and entropy generation. A higher Nr leads to a noticeable increase in the fluid velocity in the boundary layer. This is because stronger thermal radiation makes more thermal energy in the fluid,

and then reduces the resistance of the fluid and thus inducing motion near the wall. An additional temperature profile also displays a substantial increase for higher Nr. The added radiative heating in the system increases the global thermal energy of the environment, causing an enhanced thickness of thermal boundary layers and warmer temperature values everywhere (region). On the contrary, the concentration is lowered at increasing Nr. Higher wall heat fluxes associated with radiation generally lead to enhanced diffusion of species away from the wall, resulting in a decrease in concentration near the wall. The entropy production Be increases with Nr. This is due to an increase in the thermal gradients in the flow that results in higher irreversibilities within the system.

4. Conclusions:

Based on the numerical simulations and parametric analysis carried out in the present study, the key physical and thermodynamic implications of the flow are summarized below. The following conclusions highlight the dominant effects of the governing parameters on momentum, heat, and mass transfer characteristics, as well as on entropy generation and irreversibility distribution. These findings provide useful guidance for optimizing transport processes in practical engineering and energy-related applications.

- Lorentz and friction forces, which are created by the applied magnetic field and porous medium effects, oppose the velocity (heat) transfer due to strong coupling between momentum transport and heat transfer, leading to skin friction (Nusselt number) reduction, Sherwood number decrement, as well as a diminution in entropy generation rate but an augmentation of Bejan number.
- Viscosity parameter and buoyancy ratio parameters have a significant influence on the momentum, heat, and solutal transport enhancement, but it is associated with an enhanced entropy generation rate and reduced Bejan number, indicating the predominance of fluid friction irreversibility.
- Reducing the Casson fluid parameters reduces the wall shear stress and increases heat and mass transfer rates moderately, thus leading to an increase in entropy generation rate while decreasing the Bejan number.
- Thermal radiation strongly improves the rate of heat transfer and weakly increases the entropy generation rate; however, mass diffusion parameters affect mostly on Sherwood number with scant effect on heat transfer rates and irreversibility distribution.
- Brinkman and Eckert numbers play a significant role in heat dissipation when performing the thermodynamic study, as it largely enhances viscous dissipation work, entropy production rate, and control fluid friction irreversibility.
- The results apply to the study of transport phenomena and irreversibility in magnetohydrodynamic non-Newtonian fluid flow through porous media.

5. Nomenclature:

u, v : Velocity components in x and y directions [m s^{-1}]
x : Direction along the surface [m]
y : Direction normal to the surface[m]
r : Radius of the cone[m]
B_0 : Dimensional magnetic field parameter
g : Acceleration due to gravity[m s^{-2}]
k : Thermal conductivity [W m^{-1} K^{-1}]
T : Temperature of the fluid [K]
T_0 : Reference temperature[K]
T_∞ : Temperature of the fluid in free stream [K]
C : Concentration of the fluid [kg m^{-3}]
C_f : Skin friction coefficient
C_p : Specific heat capacity at constant pressure [J kg^{-1} K^{-1}]
C_0 : Reference concentration [kg m^{-3}]
C_∞ : Concentration of the fluid in free stream
D_B : Mass diffusivity [$m^2 s^{-1}$]

f : Dimensionless velocity
Sc : Schmidt number
M : Magnetic field parameter
Nu_x : Local Nusselt number
Pr : Prandtl number
Gr : Grashof number

Ec : Eckert number

Br : Brinkmann number

q_w : Surface heat flux [W m^{-2}]

j_w : Mass heat flux [kg m^{-2} s^{-1}]

Sh_x : Local Sherwood number

Greek Symbols

α : Thermal diffusivity [m^2 s^{-1}]

η : Similarity variable

ϕ : Dimensionless concentration

σ : Electrical conductivity of the fluid [S m^{-1}]

β : Thermal expansion coefficient [K^{-1}]

β^* : Mass expansion coefficient [kg m^{-3}]$^{-1}$

ω : Cone apex angle [rad]

θ : Dimensionless temperature

ρ : Density of the fluid [kg m^{-3}]

μ : Dynamic viscosity [kg m-1 s-1]

υ : Kinematic viscosity [m^2 s^{-1}]

δ : Casson parameter

τ_w : Surface shear stress [N m^{-2}]

6. References:

[1] I. Pop and T. Y. Na, "Natural convection from a wavy cone," *Applied Scientific Research*, vol. 54, no. 2, pp. 125–136, 1995, doi: 10.1007/BF00864369.

[2] C. S. K. Raju, S. Naramgari, and M. S. Jagadeesh Kumar, "Heat transfer in MHD nanofluid flow over a cone and plate in the presence of heat source/sink," *Journal of Computational and Applied Research in Mechanical Engineering*, vol. 7, no. 2, p. 253, 2018, doi: 10.22061/jcarme.2017.637.

[3] G. M. Moatimid, M. A. A. Mohamed, and K. Elagamy, "A Casson nanofluid flow within the conical gap between rotating surfaces of a cone and a horizontal disc," *Sci Rep*, vol. 12, no. 1, pp. 1–21, 2022, doi: 10.1038/s41598-022-15094-w.

[4] I. Holloway and S. S. Sritharan, "Numerical solution of compressible Euler and Magnetohydrodynamic flow past an infinite cone," *Applications in Engineering Science*, vol. 6, no. April, p. 100048, 2021, doi: 10.1016/j.apples.2021.100048.

[5] D. S. Swetha, K. R. Madhura, Babitha, I. A. Badruddin, S. Kamangar, and A. A. Khan, "MHD Maxwell nanofluid flow over a porous conical surface: A fractional approach," *Results in Engineering*, vol. 26, Jun. 2025, doi: 10.1016/j.rineng.2025.104853.

[6] M. Gouse, A. Bég, and V. Varma, "Numerical study of free convective MHD flow past a vertical cone in non-Darcian porous media," *Theoretical and Applied Mechanics*, vol. 41, no. 2, pp. 119–140, 2014, doi: 10.2298/tam1402119g.

[7] E. Ragulkumar, G. Palani, P. Sambath, and A. J. Chamkha, "Dissipative MHD free convective nanofluid flow past a vertical cone under radiative chemical reaction with mass flux," *Sci Rep*, vol. 13, no. 1, pp. 1–13, 2023, doi: 10.1038/s41598-023-28702-0.

[8] W. Abbas, M. A. Ibrahim, O. Mokhtar, A. M. Megahed, and A. A. M. Said, "Numerical Analysis of MHD Nanofluid Flow Characteristics with Heat and Mass Transfer over a Vertical Cone Subjected to Thermal Radiations and Chemical Reaction," *Journal of Nonlinear Mathematical Physics*, vol. 30, no. 4, pp. 1540–1566, 2023, doi: 10.1007/s44198-023-00142-4.

[9] M. Fathy and E. A. Sayed, "Thermal radiation effects on nanofluid flow over a vertical cone in the presence of pressure work," *Sci Rep*, vol. 15, no. 1, Dec. 2025, doi: 10.1038/s41598-025-10554-5.

[10] S. Rao and P. N. Deka, "A study on MHD flow of SWCNT-Al2O3/water hybrid nanofluid past a vertical permeable cone under the influence of thermal radiation and chemical reactions," Numer Heat Transf A Appl, vol. 85, no. 10, pp. 1591–1611, 2024, doi: 10.1080/10407782.2023.2207731.

[11] S. A. G. A. Shah, A. Hassan, H. Karamti, A. Alhushaybari, S. M. Eldin, and A. M. Galal, "Effect of thermal radiation on convective heat transfer in MHD boundary layer Carreau fluid with chemical reaction," *Sci Rep*, vol. 13, no. 1, Dec. 2023, doi: 10.1038/s41598-023-31151-4.

[12] L. J. Sademaki, B. P. Reddy, and P. M. Matao, "Thermophoresis and Brownian motion impact on diffusional heat generating MHD Jeffrey nanofluid over an inclined vertical cone with reactive species," Discov Appl Sci, vol. 7, no. 10, 2025, doi: 10.1007/s42452-025-06840-6.

[13] E. Ragulkumar, P. Sambath, A. S. V. Ravi Kanth, and S. Noeiaghdam, "MHD radiative nanofluid flow past an upright cone under the influence of dissipative chemical reactions with heat source/sink and mass flux," Mod Phys Lett B, vol. 39, no. 32, p. 2550171, 2025, doi: 10.1142/S0217984925501714.

[14] B. Rushi Kumar and R. Sivaraj, "Heat and mass transfer in MHD viscoelastic fluid flow over a vertical cone and flat plate with variable viscosity," *Int J Heat Mass Transf*, vol. 56, no. 1–2, pp. 370–379, Jan. 2013, doi: 10.1016/j.ijheatmasstransfer.2012.09.001.

[15] G. Palani, E. J. Lalith Kumar, and K. Y. Kim, "Free convection effects on a vertical cone with variable viscosity and thermal conductivity," *Journal of Applied Mechanics and Technical Physics*, vol. 57, no. 3, pp. 473–482, May 2016, doi: 10.1134/S0021894416030111.

[16] M. Y. Malik, H. Jamil, T. Salahuddin, S. Bilal, K. U. Rehman, and Z. Mustafa, "Mixed convection dissipative viscous fluid flow over a rotating cone by way of variable viscosity and thermal conductivity," *Results Phys*, vol. 6, pp. 1126–1135, 2016, doi: 10.1016/j.rinp.2016.11.027.

[17] G. C. Hazarika, B. Phukan, and S. Ahmed, "Effect of Variable Viscosity and Thermal Conductivity on Unsteady Free Convective Flow of a Micropolar Fluid Past a Vertical Cone," *Journal of Engineering Physics and Thermophysics*, vol. 93, no. 1, pp. 178–185, Jan. 2020, doi: 10.1007/s10891-020-02106-7.

[18] Z. Mustafa, T. Javed, T. Hayat, and A. Alsaedi, "Unsteady nanofluid flow over a cone featuring mixed convection and variable viscosity," *Heliyon*, vol. 9, no. 6, Jun. 2023, doi: 10.1016/j.heliyon.2023.e16393.

[19] H. B. Keller, " A new difference scheme for parabolic problems. In Numerical Solution of Partial Differential Equations–II; Elsevier: Amsterdam, The Netherlands, 1971; pp. 327–350".

[20] S. Rehman, N. Hashim, S. B. H. Hassine, E. Tag Eldin, and S. O. Shah, "Investigation of Entropy Production with Thermal Analysis under Soret and Dufour Effects in MHD Flow between Convergent and Divergent Channels," *ACS Omega*, vol. 8, no. 10, pp. 9121–9136, Mar. 2023, doi: 10.1021/acsomega.2c05937.

[21] P. R. Tangsali, N. N. Katagi, A. Bhat, and M. Shettar, "Keller-box method analysis of MHD micropolar fluid flow in a porous duct with stretching walls and slip conditions," *Cogent Eng*, vol. 12, no. 1, 2025, doi: 10.1080/23311916.2025.2555355.

Paper submitted: 13.04.2026.
Paper revised: 20.08.2026.
Paper accepted: 31.08.2026.